Dalton Transactions

An international journal of inorganic chemistry

Accepted Manuscript

This article can be cited before page numbers have been issued, to do this please use: S. Tandon, M. Venkatesan, W. Schmitt and G. W. Watson, *Dalton Trans.*, 2020, DOI: 10.1039/D0DT01404D.

ROYAL SOCIETY OF CHEMISTRY

rsc.li/dalton

View Article Online
DOI: 10.1039/D0DT01404D

ARTICLE

Altering the nature of coupling by changing the oxidation state in a {Mn_6} cage

Received 00th January 20xx,
Accepted 00th January 20xx

DOI: 10.1039/x0xx00000x

Swetanshu Tandon,*[a,b] Munuswamy Venkatesan,[c] Wolfgang Schmitt*[a,b] and Graeme W. Watson*[a]

Polynuclear transition metal complexes have continuously attracted interest owing to their peculiar electronic and magnetic properties which are influenced by the symmetry and connectivity of the metal centres. Understanding the full electronic picture in such cases often becomes difficult owing to the presence of multiple bridges between metal centres. We have investigated the electronic structure of a {Mn_6} cage complex using computational and experimental approaches with the aim to understand the coupling between the manganese centres. The nature of the various coupling pathways has been determined using a novel methodology that involves perturbing the system while retaining the symmetry and analysing the effect on the coupling strength due to the perturbation. Furthermore, we have investigated the magnetic properties of this complex in higher oxidation states which reveals a switch in the nature of coupling from antiferromagnetic to ferromagnetic in addition to stabilisation of intermediate spin states.

Introduction

Polynuclear manganese complexes have attracted a lot of attention because of their interesting electronic and magnetic properties such as colossal magnetoresistance,[1] ferroelectricity[2] and single molecule magnetism,[3] the last one being a major driving force. The first reported single molecule magnet (SMM) was a {Mn_{12}} complex which had a blocking temperature of 2K.[4] Since the energy barrier for this blocking temperature is proportional to the total number of unpaired electrons, there has been a large variety of transition metal based polynuclear complexes synthesised with the aim of obtaining a large total spin value.[5] Mn complexes have generally topped the list for the largest spin ground state among transition metal complexes and for a long time, the system with the highest ground spin state was a {Mn_{19}} complex (S = 83/2)[5f] which has been recently succeeded by an {Fe_{42}} system (S = 90/2).[5i]

Mn complexes have also been studied extensively as catalysts for various reactions,[6] the oxygen evolution half-reaction of water splitting being a key one. This is because the catalyst used by nature for accomplishing the oxidation half-reaction of water splitting is a mixed metal {Mn_4Ca} complex found in photosystem-II.[6d, 7] It has been observed that the nature of exchange coupling between metal centres can have a significant impact on the kinetics of the reaction.[8] McGrady et al. investigated the cleavage of the O_2 bond by a Mn dimer. They found that the antiferromagnetic coupling between the Mn centres is more favourable for the formation of the O-O σ bond while ferromagnetic coupling is more favourable for the formation of the O-O π bond. The nature of coupling between metal centres thus affects the kinetic barrier to bond formation/cleavage.[8a] The kinetics of this reaction can therefore be modified if one can have antiferromagnetically coupled metal centres for the formation of O-O σ bond which can switch to being ferromagnetically coupled for the formation of the O-O π bond.

In polynuclear complexes, metal centres are generally bridged together by multiple ligands. This implies that the observed exchange coupling strength between the metal centres is a sum of coupling via all the bridges. To fully understand the coupling in a polynuclear complex, one therefore needs to identify the effect of each ligand bridge on the coupling. The approaches currently used to achieve this include the variation of geometrical parameters of the system under study, the substitution of paramagnetic centres with diamagnetic centres and the use of the overlap matrix.[9] These approaches however, become increasingly complicated for larger systems.

In this study, we have investigated, both experimentally and computationally, the magnetic properties of the [Cl⊂Mn^{III}_6(*tert*-butyl-PO_3)$_8$(4-picoline)$_6$]Cl cage complex (Fig. 1) previously reported by us.[5j, 10] Using hybrid density functional theory (DFT), we have examined this complex in five oxidation states to understand the nature of coupling between the Mn centres in the different oxidation states and to examine the possibility of switching the coupling during the oxidation process. We have also determined the mechanism of exchange coupling between Mn centres via different bridges using a novel methodology.

[a] School of Chemistry & CRANN Institute, University of Dublin, Trinity College, Dublin 2, Ireland.
[b] AMBER Centre, University of Dublin, Trinity College, Dublin 2, Ireland.
[c] School of Physics & CRANN Institute, University of Dublin, Trinity College, Dublin 2, Ireland.
Email: schmittw@tcd.ie, tandons@tcd.ie, watsong@tcd.ie

† Electronic Supplementary Information (ESI) available: [Fig. S1.1-8.1, Table S2.1-8.1 and description of the 3rd and the 4th charged states]. See DOI: 10.1039/x0xx00000x

View Article Online
DOI: 10.1039/D0DT01404D

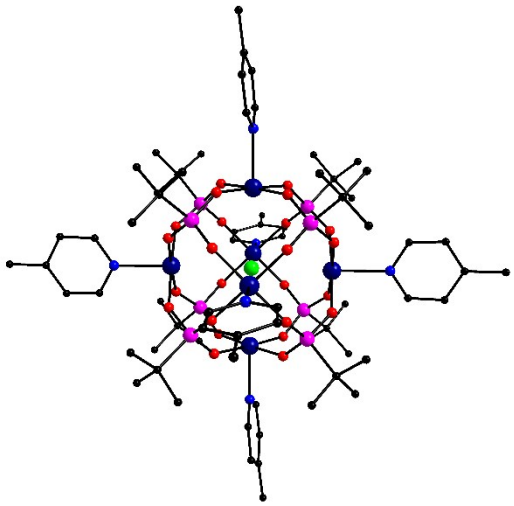

Fig. 1: Structure of the {Mn_6} model, $[Cl\subset Mn^{III}_6(tert\text{-butyl-}PO_3)_8(4\text{-picoline})_6]^+$.[10] Colour scheme: Mn (dark blue), P (pink), Cl (green), C (black), N (blue) and O (red). Hydrogen atoms have been removed for clarity.

Experimental

General comments

All reagents were bought from Sigma-Aldrich and were used without further purification. The elemental analyses data was obtained from the Microanalysis lab, School of Chemistry and Chemical Biology, University College Dublin. Magnetic susceptibility measurements were performed using a 5-Tesla Quantum Design MPMS 5T SQUID magnetometer.

Synthesis of $[Cl\subset Mn^{III}_6(tert\text{-butyl-}PO_3)_8(4\text{-picoline})_6]Cl$: The reported procedure[10] was followed for the synthesis of this compound. A mixture of $MnCl_2.2H_2O$ (0.162 g, 1.0 mmol), $KMnO_4$ (0.032 g, 0.2 mmol), tert-butylphosphonic acid (0.136 g, 1.0 mmol), 1,4-phenylenediacetic acid (0.193 g, 1.0 mmol) and 4-picoline (0.24 ml) in CH_3CN (25 ml) was stirred at room temperature for 5 hours. The resultant solution was filtered and the filtrate was left undisturbed at room temperature for slow evaporation. Crystals were obtained within a few weeks. The crystals obtained this way were dissolved in $CHCl_3$ which was allowed to evaporate. The resultant precipitate was recrystallised using minimum volume of CH_3CN and 0.20 ml of 4-picoline. Elemental analysis ($C_{68}H_{114}Cl_2Mn_6N_6O_{24}P_8$): Calculated (%) – C 39.88, H 5.61, N 4.10; found (%) – C 39.22, H 5.63, N 3.91. The compound was further characterised using powder X-ray diffraction and infrared spectroscopy (Fig. S1.1 and S1.2, ESI†).

Computational Methodology

All calculations have been carried out using the cluster codes gaussian09[11] and ORCA 3.0.3.[12] The hybrid PBE0 functional[13] has been used in conjunction with the SDDALL[14] basis set having an effective core potential for the Mn atoms (replacing the 10 core electrons – $1s^22s^22p^6$ – of Mn with fully relativistic pseudopotentials), the 6-31G(d)[15] basis set for O, C and N, 6-31G(2d)[16] basis set for phosphorus and chlorine and 6-31G(p)[15] basis set for H.

In the fully reduced state, all Mn centres are in oxidation state III. For the higher charged states, electrons were removed such that no Mn centre has an oxidation state greater than IV. For all five oxidation states, the optimisation of the ferromagnetic configurations was performed using the berny optimiser[17] as implemented in gaussian09.[11] The default convergence criteria and a large grid containing 225 radial shells with each shell containing 974 angular points were used.

For modelling the non-ferromagnetic configurations, broken symmetry calculations[18] were performed. For these, the corresponding ferromagnetic state was used as the initial guess. The wavefunction was then analysed to look for instabilities[19] and optimised until a stable wavefunction was found. This wavefunction was then employed for the final geometry optimisation using the berny optimiser.[17]

The exchange coupling constants (J-values) were calculated using the Heisenberg Dirac van Vleck Hamiltonian:[20]

$$\hat{H} = -2\sum_{i>j} J_{ij} S_i S_j \qquad \text{(eq. 1)}$$

where J_{ij} is the coupling constant between the magnetic centres i and j, and s_i and s_j are the spin operators for the centres i and j which were defined using the atomic spin density which has been shown to give results comparable to those obtained using the spin projection method.[21] The spin density has been expressed in a number of ways which includes the use of formal spins, Mulliken, Hirshfeld and Bader charge analyses.[22]

The energy obtained from the DFT calculations includes the energy associated with interactions other than the exchange coupling. To determine the energy changes associated with coupling of the Mn centres, one can assume that the energy of different spin configurations differs only by this amount and use one of the states as a reference. Once, the reference equation has been selected, the problem at hand is to solve a set of n simultaneous linear equations with n unknowns (coupling constants). Thus, to obtain n coupling constants, (n+1) spin configurations need to be modelled.

If there are x paramagnetic centres, there can be a maximum of x(x-1)/2 coupling constants and a total of 2^x different spin configurations. The presence of symmetry may decrease the number of unique coupling constants and spin configurations. For the fully reduced state of the {Mn_6} cage one can have a maximum of (6(6-1)/2 =) 15 coupling constants while the total number of spin configurations for this complex is (2^6 =) 64. Out of these 64 configurations, 32 are mirror images of the other 32 configurations based on the spin orientation. For example, the configuration with all unpaired electrons spin up is identical to the one where all unpaired electrons are spin down.

Despite the need to model only n+1 states for the determination of n coupling constants,[9b, 9h, 23] the option of modelling more states has been explored in recent studies to remove any dependence of the coupling constants on the choice of spin state modelled.[9e, 9f, 9l, 9m] We have used a similar approach and modelled extra states for each oxidation state.

View Article Online
DOI: 10.1039/D0DT01404D

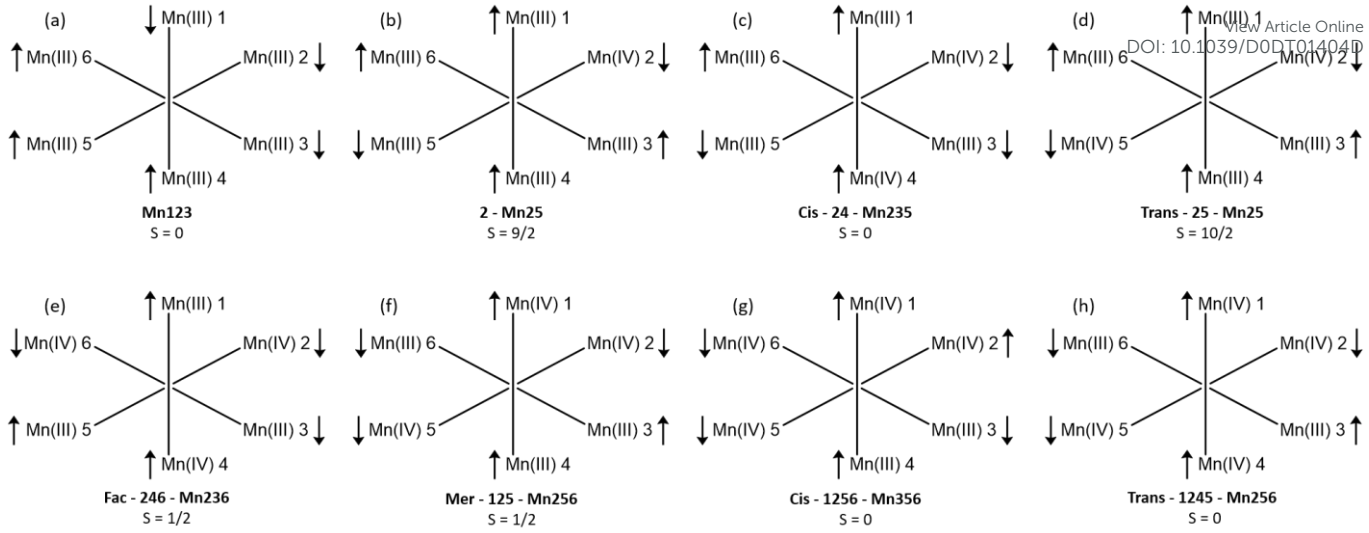

Fig. 2: Arrangement of Mn atoms and their spins in the $\{Mn_6\}$ cage in the ground electronic state of the various charged states. The numbers before 'Mn' in the labels below each state specify which Mn centres are in +IV oxidation state while the numbers after 'Mn' specify which Mn centres have a down spin. The prefix (*cis*/*trans* or *fac*/*mer*) specifies the arrangement of Mn(IV) centres in the model for the 2nd and 3rd charged states and that of Mn(III) atoms in the 4th charged state. e.g. ***Cis*– 24 – Mn235** state represents the state where Mn2 and Mn4, which are cis- to each other, are in oxidation state IV and Mn2, Mn3 and Mn5 have down spin.

This implies that more than one set of coupling constants exists, i.e. the solution is overspecified and so, we have calculated all possible solutions. When calculating *r* coupling constants using *n* spin configurations (where $n > r$), there are $n[(n-1)!/\{r!\,(n-1-r)!\}]$ sets of solutions obtained. Out of these, the ones which were found to be singular were discarded and the average and the standard deviation for each coupling constant were determined. The solutions in which any of the coupling constant deviated by more than three standard deviations were discarded and the average and standard deviation were re-calculated with the cycle repeated until self-consistency.

Once the coupling constants were obtained, they were used to determine the energy associated with the different spin configurations for all 32 possible electronic states using the Heisenberg Dirac van Vleck Hamiltonian (eq. 1). The spin density on each Mn centres was determined by taking an average of the spin densities in the different electronic states that were modelled. This procedure of calculating the coupling constants and determining the ground electronic state has been implemented in the code ej_calc.[24]

To account for the effects of the applied magnetic field and calculate the magnetic susceptibility, the Zeeman term needs to be added to the Hamiltonian in eq. 1 as follows:[25]

$$\hat{H} = -2\sum_{i>j} J_{ij} S_i S_j + g\mu_B B \sum_i S_i \qquad \text{(eq. 2)}$$

where g is the g-tensor, μ_B is the Bohr magneton and B is the applied magnetic field. The g-tensor was calculated for the ferromagnetic configuration of the corresponding charged state with ORCA 3.0.3.[12, 26] For this calculation, grid 7 was employed along with the same basis set and functional as used in gaussian09. The calculation of magnetic susceptibility and fitting of coupling constants to the susceptibility were carried out using the PHI code developed by Chilton et al[27] and an in-house code suscep.[28]

Results and discussion

We have investigated the electronic structure of the $\{Mn_6\}$ cage[10] in 5 oxidation states. In the fully reduced state it is positively charged and comprises of 6 Mn(III) centres which reside at the vertices of an octahedron centred around a Cl^- ion (Fig. 1). The system is stabilised by 8 *tert*-butyl phosphonate groups which fulfil 4 out of the 6 coordination sites for each Mn(III) centre, and any two Mn centres *cis*- to each other are connected to each other by two phosphonate groups. The Mn centres are additionally coordinated to the N-donor of the 4-picoline ligands. The Jahn-Teller axis of all the Mn(III) centres is directed along the Mn(III)-Cl bond.

Ground state configurations

In the fully reduced state, the **Mn123** state (the configuration in which the Mn centres Mn1, Mn2 and Mn3 have down spin), with S = 0, was found to be the ground electronic state (Fig. 2a). To oxidise this system, an electron was removed from Mn2. The Jahn-Teller axis of Mn(III) centres remains directed towards the centre of the cage upon oxidation and redirecting it was found to be unfavourable. This oxidation gives rise to the **2 - Mn25** (S = 9/2) ground state in which Mn2 is in oxidation state IV and Mn2 and Mn5 have down spin (Fig. 2b). An S = 1/2 state does not form the ground state as may have been expected. This indicates that the oxidation of the system leads to a change in not only the strength but also the nature of interactions between Mn centres.

Further oxidation presents two possibilities as the additional charge can be accommodated by the cage in a manner such that the two Mn(IV) centres are *cis*- or *trans*- to each other. The *cis*-isomer has been found to be more stable by ~19 kJ/mol. The ground electronic state for the two isomers have been found to be different. ***Cis* - 24 - Mn235** with S = 0 and ***trans* - 25- Mn25** with S = 10/2 form the ground state for the *cis*- and *trans*-

View Article Online
DOI: 10.1039/D0DT01404D

isomer respectively (Fig. 2c and 2d), where the prefix *cis*- and *trans*- highlights the fact that the Mn(IV) centres are *cis*- or *trans*- to each other.

The oxidation to the third and fourth charged state also leads to two isomers each. The *fac*/*cis*- isomer for the third and fourth charged state (Fig. 2e and g) is more stable (~3 and ~9 kJ/mol respectively) although the stabilisation energy is lower compared to the second charged state. For both *fac*- and *mer*- isomers of the third charged state, S = 1/2 states form the ground state. Similarly, for the *cis*- and *trans*- isomer of the fourth charged states, the lowest spin states (S = 0) are the most stable (Fig. 2e-h).

To understand these changes in the electronic configuration on oxidation, we need to understand how the Mn centres couple. In the following we describe the fully reduced state, compare the results with experiment, and investigate the coupling mechanism via each bridge. This is followed by a description of the higher charged states to explain the changes in the spin multiplicity of the ground electronic state during successive oxidation.

Coupling constants of the fully reduced state

The structural features of the cage were modelled with less than 2% difference in the key bond lengths and bond angles in comparison to the experimental crystal structure[10] (Table S2.1, ESI†). The *trans*- Mn-Mn distances are 6.19 Å in the ferromagnetic state with the corresponding distances for the other spin states found to be within ±0.01 Å. The value of g-tensor has been found to be 1.998 for the ferromagnetic configuration of this state.

Six unique spin configurations were identified for the fully reduced state including the ferromagnetic state which was found to be the highest in energy (Fig. 3). The Jahn-Teller axis of all the Mn(III) centres is along the Mn(III)-Cl bond in all the six configurations. Bader analysis predicts that the spin density on each Mn centre is approximately 3.8 (Table S2.3, ESI†) indicating strong localisation. The sum of spin density on the O-donors of the phosphonate group attached to each Mn centres is ~0.085 while that on the Cl is 0.116 (Table S2.8, ESI†).

Due to the symmetry of the system, one can expect that two coupling constants – one for the coupling between Mn centres *cis*- to each other (J_{cis}) and the other for the ones *trans*- to each other (J_{trans}) – should be sufficient to describe the magnetic behaviour of the system as follows:

$$\begin{aligned} H = -2J_{trans}[&\langle s_1.s_4\rangle + \langle s_2.s_5\rangle + \langle s_3.s_6\rangle] \\ &- 2J_{cis}[\langle s_1.s_2\rangle + \langle s_1.s_3\rangle \\ &+ \langle s_1.s_5\rangle + \langle s_1.s_6\rangle \\ &+ \langle s_2.s_3\rangle + \langle s_2.s_4\rangle \\ &+ \langle s_2.s_6\rangle + \langle s_3.s_4\rangle \\ &+ \langle s_3.s_5\rangle + \langle s_4.s_5\rangle \\ &+ \langle s_4.s_6\rangle + \langle s_5.s_6\rangle] \end{aligned} \qquad \text{(eq. 3)}$$

Considering the large distance between the *trans*-Mn centres, the possibility that one coupling constant (J_{cis}) may prove sufficient cannot be ignored. Additionally, since Mn centres *cis*- to each other can also be divided into two groups based on the Mn-Mn distances (4.41 and 4.39 Å – see Table S2.2, ESI†), there is a possibility that 3 coupling constants will be needed.

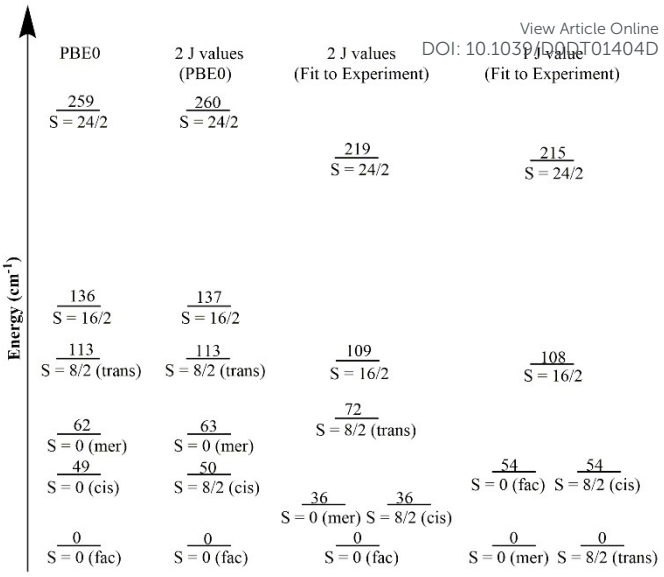

Fig. 3: Relative energies of the 6 spin states of the $\{Mn_6\}$ cage obtained using DFT (PBE0), and the calculated and fitted J-values.

Examination of the three possibilities suggests that the 2 J-value model is the most appropriate as the 1 J-value model leads to inconsistent solutions while the values obtained with the 3 J-value model are within the standard deviation for the values obtained with the 2 J-value model (Table S2.10, ESI†). With the 2 J-value model, the average coupling constants obtained using Bader spin densities are provided in Table 1. The values obtained using other charge analysis schemes and the spin projection method[29] were found to be similar (Table S2.9, ESI†). These J-values were used to determine the energy associated with the different spin configurations for all 6 states and have been found to be in agreement with the DFT results (Fig. 3).

PBE0 has been previously shown to provide good estimates of magnetic properties.[30] Since, we are using calculated spin densities to define the spin operators, PBE0 is better suited than most other DFT functionals since it has been shown to reproduce the electron density quite accurately.[31] The functional dependence has still been tested using B3LYP and results similar to those obtained with PBE0 were obtained (Table S2.12, ESI†).

Table 1: Calculated J values (using Bader charge densities) and fitted J-values for the $\{Mn_6\}$ cage.

Approach\J value	J_{trans} (cm^{-1})	J_{cis} (cm^{-1})
Calculated (PBE0)	-3.48 ± 0.05	-1.28 ± 0.04
Fit to Experiment (2 J-values)	-2.53	-1.28
Fit to Experiment (1 J-value)	-	-1.88

To further assess the validity of the coupling constants, the effect of temperature on the magnetic susceptibility has been calculated and compared with the experimental data. For this purpose, we synthesised the cage and measured the magnetic susceptibility (Fig. 4) which was found to be similar to that which has been reported previously.[10] This was then compared with the magnetic susceptibility obtained using the calculated

View Article Online
DOI: 10.1039/D0DT01012D

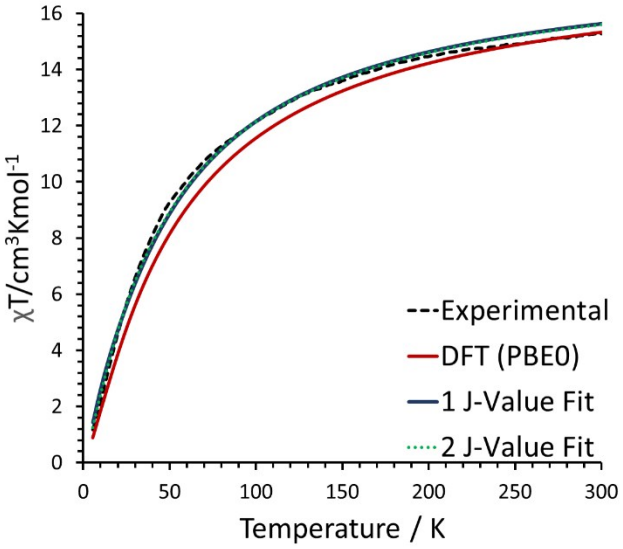

Fig. 4: Experimental χT vs T plot for the {Mn_6} cage and the same plot obtained using the calculated (PBE0) and fitted coupling constants.

coupling constants (Fig. 4) and it can be seen that the experimental and calculated plots are slightly different. We performed a 2 coupling constant fit to the experimental plot and the values corresponding to the best fit are given in Table 1. J_{cis} has been found to be identical to that calculated using DFT while J_{trans} differs from the calculated one by ~1 cm^{-1}. For comparison, we also fitted only 1 coupling constant (J_{cis}) to the experimental curve (Table 1) and it can be seen that it reproduces the experimental curve reasonably (Fig. 4). The residual error, as calculated using phi,[27] for these 1 and 2 J-values fits were found to be 19.4 and 12.2 respectively which shows that the curve obtained from 1 J-value is inferior to that obtained using 2 J-values as was expected.

To investigate how these J-values fitted to the experimental data reproduce the electronic picture of the cage, they were used to calculate the relative energies of the 6 spin states. For this purpose, we calculated the energies of each spin configuration using equation 3, the J-values fitted to the experimental data and the s_i values obtained from the Bader spin densities of our DFT calculations. It can be seen from Fig. 3 that with the 2 J-values fitted to the experimental data, the relative energy of the states follow the same order as the DFT results. The ground state is correctly predicted and the next two states, S = 8/2 (*cis*) and S = 0 (mer), are predicted to be close in energy by DFT (13 cm^{-1} apart) but are almost degenerate with the 2 J-values fitted to the experimental data. All of the other states are in the correct order although the spacing is slight smaller than that found with DFT. It can also be seen that when only one J-value is fitted to the experimental data, the ground state is incorrectly predicted even though the susceptibility curve is reasonably reproduced. This suggests that one needs to be cautious when trying to fit coupling constants to magnetic susceptibility curves and ensure that the complete electronic picture is captured.

Table 2: Coupling constants for the fully optimised {Mn_6Cl} and partially optimised {Mn_6}.

	J_{trans}	J_{cis}
{Mn_6} with Cl (optimised)	-3.48 ± 0.05	-1.28 ± 0.04
{Mn_6} without Cl (constrained)	-0.03 ± 0.02	-1.40 ± 0.01

Mechanism of coupling between Mn centres

The Mn centres *trans*- to each other can only be coupled via the Cl bridge. The negative J_{trans} value indicates that the coupling pathway between the *trans*-Mn centres must be antiferromagnetic which is in line with Goodenough-Kanamori-Anderson rules.[32] The Mn centres *cis*- to each other, on the other hand, can be coupled by both the phosphonate and the Cl bridge. In this case, both pathways may be antiferromagnetic or only the dominant one may be antiferromagnetic.

To investigate the coupling mechanism between the *cis*-Mn centres via the different bridges, we employed an innovative approach that involves perturbing the system while retaining the symmetry and analysing the effect on the coupling strength due to the perturbation. To our best knowledge this is the first study employing this methodology. The perturbation can be introduced by removing bridges or by substituting the bridging groups with their heavier/lighter analogues. Here, we removed the Cl from the centre, and optimised the same 6 spin configurations. The coupling constants were obtained using the 2 J-value Hamiltonian (eq. 3) and are shown with the original coupling constants in Table 2.

J_{trans} is effectively zero due to absence of the Cl bridge which ascertains the absence of any direct *trans*- coupling between Mn centres and further confirms that they are coupled antiferromagnetically and through the Cl bridge. J_{cis} retains its sign but increases slightly. Since the coupling is now only via the phosphonate bridge, it indicates that this pathway is antiferromagnetic. Additionally, since J_{cis} is greater in the absence of the Cl coupling pathway, it suggests that the Cl pathway is weakly ferromagnetic.

To validate our methodology, we investigated the overlap of the d-orbitals of Mn centres with the p-orbitals of the Cl in our parent model with the central Cl present (Table S2.13, ESI†). The interaction between the Mn centres *trans*- to each other via the Cl was found to be of σ type which indicates that the coupling will be antiferromagnetic. The d-orbitals of Mn centres cis- to each other overlap with orthogonal p-orbitals on Cl. Since the p-orbitals are orthogonal, the coupling will be indirect through the interaction of the orthogonal p-orbitals on the Cl and hence ferromagnetic[32] which is consistent with our predictions.

Charged states

In these states, the oxidation has been achieved by introducing Mn(IV) sites and in cases where the Mn(IV) centres can be *cis*- or *trans*- to each other, both have been analysed. All bond distances reported (irrespective of the charged state under consideration) correspond to those of the ferromagnetic configuration because, similar to fully reduced state, the bond distances of other spin configurations do not vary significantly. For defining the spin operators in the higher charged states we have only used Bader spin densities. The spin densities reported

in the following discussion are the ones for the ferromagnetic state. The value of the g-tensor for these states was found to be 1.997 ± 0.001, decreasing with increasing charge (Table S3.1, ESI†).

1st charged state

In this charged state, Mn2 is in oxidation state IV (Fig. 2b). The Mn1-Mn4 and Mn3-Mn6 distances have been found to be 6.332 Å while the Mn2-Mn5 distance has been found to be 6.129 Å which means that the cage expands on oxidation. Cl shifts towards Mn2, because of its higher oxidation state (Table S3.2, ESI†).

The electronic environment of Mn5(III) can be considered different from all other Mn(III) centres since it is *trans*- to Mn2(IV) which itself resides in a unique electronic environment owing to its oxidation state. Keeping this in mind, the coupling behaviour can be captured using 5 J-values as shown in Table 3. To calculate these, 16 spin configurations were modelled (Table S4.1, ESI†) and the J-values thus obtained were found to reproduce the relative energies of all 15 states well (< 3% error). The coupling between Mn2(IV) and Mn5(III) (J_1), unlike the fully reduced state, is ferromagnetic. Oxidation of this system from the fully reduced state, thus leads to a switch in the nature of coupling from antiferromagnetic to ferromagnetic. All other Mn pairs are antiferromagnetically coupled. There is, thus, a competition between ferromagnetic and antiferromagnetic coupling which affects the energy of the different spin configurations and enables the **2 – Mn25** (S = 9/2) state to be the lowest in energy.

The ferromagnetic coupling between Mn2 and Mn5 can be explained on the basis of spin polarisation mechanism[3] which seems counter-intuitive because the spin density on Cl has the same sign as that on the Mn centres (Table S3.3, ESI†). To ascertain the presence of spin polarisation, one needs to examine the spin density on Mn2 and the N of 4-picoline ligands bound to it which have been found to be opposite to each other (3.036 and -0.075 respectively). The spin density on the Mn(III) centres and the N of 4-picoline groups bound to them are found to have the same sign (3.77 and 0.06 respectively). This suggests that both spin delocalisation and spin polarisation mechanisms are active.[3] This is further confirmed by the spin density plot which shows that Cl accommodates spin density associated with both up and down spin (Fig. 5). The spin polarisation probably arises due to the interaction of an empty d-orbital on Mn2 with one of the p-orbitals of Cl. Thus, Cl facilitates the interaction between an empty d-orbital (Mn2) and a half-filled d-orbital (Mn5) which results in ferromagnetic coupling in line with the Goodenough-Kanamori-Anderson rules.[32]

Table 3: Magnitude of J-values (cm^{-1}) and the Mn-Mn interactions that constitute each J-value for the 1st charged state.

J-value	Interacting Mn centers	Magnitude (cm^{-1})
J_1	*trans*-Mn2(IV)-Mn5(III)	1.94 ± 0.10
J_2	*trans*-Mn1(III)-Mn4(III)	-1.03 ± 0.04
	trans-Mn3(III)-Mn6(III)	
J_3	*cis*-Mn1(III)-Mn2(IV)	-3.40 ± 0.04
	cis-Mn2(IV)-Mn3(III)	
	cis-Mn2(IV) –Mn4(III)	
	cis-Mn2(IV) –Mn6(III)	
J_4	*cis*-Mn1(III)-Mn3(III)	-1.25 ± 0.04
	cis-Mn1(III)-Mn6(III)	
	cis-Mn3(III)-Mn4(III)	
	cis-Mn4(III)-Mn6(III)	
J_5	*cis*-Mn1(III)-Mn5(III)	-1.45 ± 0.03
	cis-Mn3(III)-Mn5(III)	
	cis-Mn4(III)-Mn5(III)	
	cis-Mn5(III)-Mn6(III)	

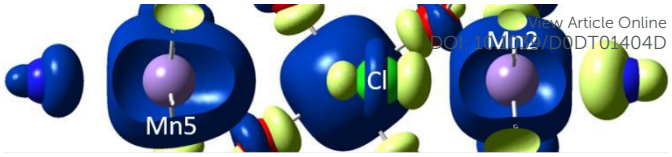

Fig. 5: Plot of the spin density distribution in the high spin configuration of the 1st charged state highlighting the spin density on Mn2 and Mn5, the N-donor bound to these Mn centres, and Cl. Purple and yellow regions represent the spin density associated with up and down spin respectively. Cl can be clearly seen to be accommodating spin density associated with both up and down spin confirming the presence of both spin delocalisation and polarisation.

As Cl serves as the only bridge between Mn2 and Mn5, the ferromagnetic coupling between Mn2 and Mn5 must be facilitated by Cl. To confirm this, the same system was modelled without the Cl in the centre. This model gives a negligible value for J_1 (Table S4.3, ESI†) confirming that the coupling between Mn2 and Mn5 is via the Cl bridge.

The coupling between the Mn(III) centres *trans*- to each other (J_2) is antiferromagnetic and is significantly weaker compared to that in the fully reduced state. This is a consequence of the cage expansion and the movement of Cl away from the centre which results in smaller Mn(III)-Cl overlaps (Table S3.4, ESI†) and hence weaker couplings.

Unlike the fully reduced state, the spin density on the O-donors of the phosphonate groups varies depending on the Mn centres they are attached to. Between any two Mn centres lie four phosphonate O-donors that are directly attached to these Mn centres. The spin density on these O-donors and the strength of the exchange coupling between the Mn centres they link are correlated with increased spin densities corresponding to stronger coupling. This can be illustrated by comparing the coupling between the *cis*-Mn(III) centres where it can be seen that $J_5 > J_4$ (Table 3). The sum of the spin densities (Table S3.3, ESI†) on the O-donors bound to Mn centres associated with J_5 is greater than those associated with J_4 which is consistent with our proposal. In addition, both J_4 and J_5 are greater than J_{cis} in the fully reduced state for which the sum of spin densities on the O-donors of the phosphonate groups is even smaller (Table S3.3, ESI†). The magnitude of spin density on the phosphonate O-donors thus provides an indication of the coupling strength between the Mn centres that they are attached to.

Despite the lower spin density on the O-donors attached to Mn2(IV) compared to those attached to Mn(III) centres, the coupling between Mn2 and its *cis*-neighbours (J_3) is stronger. This is most likely due to the higher electronegativity of Mn(IV) although the interactions via the Cl bridge could also play a role.

View Article Online
DOI: 10.1039/D0DT01404D

The latter is confirmed by the model without the Cl in the centre for which J_3 decreased to -1.63 cm^{-1} (Table S4.3, ESI†) suggesting strong antiferromagnetic coupling via the Cl bridge. Hence, for understanding the coupling strength between Mn centres one needs to take into account the oxidation state of the interacting Mn centres, the spin density on O-donors and the overlap between the orbitals of Mn and Cl.

2nd charged state

To look at whether the tendency to switch the nature of coupling is exhibited upon further oxidation, the 2nd charged state was modelled. There are two possibilities to consider in modelling this state – the two Mn centres in +IV oxiation state can either be *cis*- to each other or *trans*- to each other both of which were investigated.

***Cis*-isomer**

For the *cis*-isomer, Mn2 and Mn4 are in oxidation state IV (Fig. 2c). The *trans*-Mn(IV)-Mn(III) and Mn(III)-Mn(III) distances have been found to be ~6.182 Å and ~6.436 Å respectively. The central space containing Cl is larger compared to that in the fully reduced and the first oxidised state. Cl is shifted towards Mn2(IV) and Mn4(IV) again owing to the higher oxidation state of these Mn centres.

19 electronic configurations were modelled (Table S5.1, ESI†) and the spin Hamiltonian was found to require 12 J-values for the proper description of the electronic structure (Table 4). The relative energies of the different spin states obtained from DFT are well reproduced by these J-values (< 1.5% error). All 15 coupling constants were also calculated for this isomer (Table S5.2, ESI†) and the values obtained were found to be similar to those obtained using the 12 J-value Hamiltonian implying that the 12 J-values are sufficient.

Table 4: Magnitude of J-values (cm^{-1}) and the Mn-Mn interactions that constitute each J-value for the *cis*-isomer of the 2nd charged state.

J-value	Interacting Mn centers	Magnitude (cm^{-1})
J_1	*trans*-Mn1(III)-Mn4(IV)	1.20 ± 0.02
	trans-Mn2(IV)-Mn5(III)	
J_2	*trans*-Mn3(III)-Mn6(III)	-0.52 ± 0.03
J_3	*cis*-Mn2(IV)-Mn4(IV)	-2.13 ± 0.04
J_4	*cis*-Mn1(III)-Mn2(IV)	-2.50 ± 0.03
J_5	*cis*-Mn2(IV)-Mn3(III)	-2.04 ± 0.04
J_6	*cis*-Mn2(IV)-Mn6(III)	-2.64 ± 0.02
J_7	*cis*-Mn3(III)-Mn4(IV)	-2.76 ± 0.03
J_8	*cis*-Mn4(IV)-Mn5(III)	-2.07 ± 0.04
J_9	*cis*-Mn4(IV)-Mn6(III)	-2.40 ± 0.02
J_{10}	*cis*-Mn1(III)-Mn5(III)	-1.79 ± 0.02
J_{11}	*cis*-Mn1(III)-Mn3(III)	-1.51 ± 0.02
	cis-Mn5(III)-Mn6(III)	
J_{12}	*cis*-Mn1(III)-Mn6(III)	-1.42 ± 0.02
	cis-Mn3(III)-Mn5(III)	

The coupling between Mn(IV) centres and their *trans*- Mn(III) counterpart is again ferromagnetic (J_8) as observed for the 1st charged state. This is due to spin polarisation mechanism which is evident not only from the spin density on the N-donor of the 4-picoline bound to Mn(IV) but also the central Cl (Table S3.3, ESI†). Unlike the 1st charged state, the spin density on Cl here is opposite to that on the Mn(IV) centres because of significantly smaller overlap between the p-orbitals of Cl and the d-orbitals of Mn(III) centres (Table S3.4, ESI†). The smaller Mn(III)-Cl overlaps also result in weaker coupling between the Mn(III) centres *trans*- to each other. Additionally, the weaker coupling between Mn(IV) centres and their *cis*-Mn(III) neighbours ($J_4 - J_9$) compared to the first charged state can also be attributed to smaller Mn(III)-Cl overlaps (Table S3.4, ESI†) which decreases the contribution of the Cl bridge to the coupling.

For this configuration, the S = 0 state (***Cis* - 24 – Mn235**) has been found to be the lowest in energy and the ferromagnetic state is the highest in energy. Unlike the first oxidised state, the presence of ferromagnetic interactions does not lead to a state with higher multiplicity being the ground state.

***Trans*-isomer**

For the *trans*-isomer, Mn2 and Mn5 are in oxidation state IV (Fig. 2d) and Cl is again closer to Mn2. The Mn(IV)-Mn(IV) and Mn(III)-Mn(III) distances have been found to be 6.073 and 6.376 Å respectively suggesting further expansion of the cage compared to the 1st charged state.

11 different configurations were modelled for this state (Table S5.3, ESI†) and 8 coupling constants are required to properly describe the electronic structure (Table 5). The relative energies of the different spin states obtained from DFT are well reproduced by these J-values (< 1% error). The symmetry of this state, the spin densities on the phosphonate O-donors and the similar values of J_3 and J_4, J_5 and J_6, and J_7 and J_8 suggest that these interactions can be coupled but doing so leads to a large standard deviation on J_1 and its sign cannot be determined.

Table 5: Magnitude of J-values (cm^{-1}) and the Mn-Mn interactions that constitute each J-value for the *trans*-isomer of the 2nd charged state.

J-value	Interacting Mn centers	Magnitude (cm^{-1})
J_1	*trans*-Mn2(IV)-Mn5(IV)	0.13 ± 0.01
J_2	*trans*-Mn1(III)-Mn4(III)	-1.09 ± 0.01
	trans-Mn3(III)-Mn6(III)	
J_3	*cis*-Mn1(III)-Mn2(IV)	-3.58 ± 0.01
	cis-Mn2(IV)-Mn4(III)	
J_4	*cis*-Mn2(IV)-Mn3(III)	-3.40 ± 0.01
	cis-Mn2(IV)-Mn6(III)	
J_5	*cis*-Mn1(III)-Mn5(IV)	-1.97 ± 0.01
	cis-Mn4(III)-Mn5(IV)	
J_6	*cis*-Mn3(III)-Mn5(IV)	-1.75 ± 0.01
	cis-Mn5(IV)-Mn6(III)	
J_7	*cis*-Mn1(III)-Mn3(III)	-1.25 ± 0.01
	cis-Mn1(III)-Mn6(III)	
J_8	*cis*-Mn3(III)-Mn4(III)	-1.29 ± 0.01
	cis-Mn4(III)-Mn6(III)	

The coupling between the Mn(IV) centres is weakly ferromagnetic (J_1) and the tendency to switch the nature of coupling in this case is retained. It can be concluded that oxidation of a Mn(III) centre to Mn(IV) leads to ferromagnetic coupling between the Mn(IV) centre and its *trans*-

Mn(III)/Mn(IV) counterpart. The ferromagnetic coupling here is also due to spin polarisation as indicated by the spin density on the nitrogen of the 4-picoline ligands bound to the Mn(IV) centres. The spin density on Cl is again of the same sign as that on the Mn centres which is due to the relatively larger overlaps between the d-orbitals of Mn(III) centres and the p-orbitals of Cl compared to the *cis*-isomer (Table S3.4, ESI†).

The coupling between Mn2(IV) and its *cis*-neighbours (J_3 and J_4) is similar to that in the first charged state while the coupling between Mn5(IV) and its *cis*- neighbours (J_5 and J_6) is similar to the coupling between the Mn(IV) centres and their *cis*-neighbours in the *cis*- isomer of this charged state. This comparison highlights the importance of the Mn(IV)-Cl overlaps which is larger in the former case and smaller in the latter which results in J_3 and J_4 being larger than J_5 and J_6.

For this configuration, the ferromagnetic state is the highest in energy while the S = 10/2 state (***Trans* - 25 – Mn25**) has been found to be the lowest in energy. The 2nd charged state thus presents the possibility of two isomers where one (*cis*-isomer) has an S = 0 ground state while the other (*trans*-isomer) has an S = 10/2 ground state. Different magnetic ground states can thus be stabilised depending upon the isomer.

3rd and 4th charged state

To look at whether the tendency to stabilise intermediate spin states can be retained upon further oxidation, the 3rd and the 4th charged states were modelled. Both charged states can have two isomers each. In each case, however, the lowest spin state was found to be the ground state which suggests that the stabilisation of intermediate spin states is lost after the 2nd charged state (see ESI†). Further charged states were not modelled as the 3rd and 4th charged states failed to stabilise intermediate spin states.

Trends observed upon oxidation

The oxidation of the cage affects the coupling behaviour between the Mn centres but some general trends can be identified within all the oxidations states modelled. The coupling between *trans*-Mn centres becomes ferromagnetic if one of the Mn centres is in oxidation state IV, and the coupling is via the spin polarisation mechanism. Such a change in the nature of coupling between metal centres however, becomes very important in reactions like the O-O bond formation.[8] Systems similar to this $\{Mn_6\}$ cage with a diamagnetic ion trapped within may provide a way to catalyse such reactions effectively.

The oxidation leads to cage expansion and the central Cl moves towards the Mn(IV) centre(s) resulting in different Mn-Cl overlaps. The extent of delocalisation of the spin density from Mn centres to the bound ligand groups increases with the oxidation state and the spin density distribution on the O-donors of the phosphonate groups becomes non-uniform. The spin density on the O-donors was found to be inversely proportional to the Mn-Cl overlaps. Smaller Mn-Cl overlaps lead to greater spin density on the O-donors bound to the corresponding Mn centre. A direct consequence of the increased delocalisation is that the coupling between Mn(IV) centres *cis*- to each other and Mn(III) centres *cis*- to each other, in general, increases. When Mn(IV) centres are *cis*- to Mn(III) centres, some variation is observed in the coupling strength. In the various charged states, the *cis*-Mn(IV)-Mn(III) coupling is found to vary between -3.6 and -1.5 cm^{-1} and the variation is due to different Mn-Cl overlaps and the consequential non-uniform distribution of spin densities on the O-donors.

Conclusions

To conclude, we have computationally and experimentally probed the magnetic properties of a $\{Mn_6\}$ cage. All Mn centres in this complex are antiferromagnetically coupled to each other and the coupling can be described using two coupling constants – one for the coupling between the Mn centres *cis*- to each other while the other for those *trans*- to each other. The mechanism of coupling via both bridges was explicitly determined using a novel methodology which involves perturbing the system in such a way that the symmetry is retained and then analysing the effect of the perturbation on the coupling strength. It was found that the coupling between the *cis*-Mn centres via the Cl bridge is weakly ferromagnetic while that via the phosphonate bridge is antiferromagnetic.

The oxidation of this cage was also investigated and it was observed that the $\{Mn_6\}$ cage can potentially accommodate the loss of four electrons which is accompanied by expansion of the cage. The successive oxidation of this system gives rise to some unusual magnetic properties. The oxidation results in the movement of Cl towards the Mn(IV) centre(s). The trends in the coupling strength between Mn centres *cis*- to each can be explained by taking into account the oxidation state of the interacting Mn centres, the spin density on the O-donors of phosphonate groups and the Mn-Cl overlaps. The oxidation also leads to switching of the nature of coupling between *trans*-Mn centres from antiferromagnetic to ferromagnetic in addition to stabilisation of intermediate spin states. The latter is retained up to the second charged state but the switching occurs whenever one of the interacting *trans*-Mn centres is in oxidation state IV. Such a change can potentially allow fine tuning of reactions like the O-O bond formation where the nature of coupling between the Mn sites can affect the rate of the reaction.

Conflicts of interest

There are no conflicts to declare.

Acknowledgements

The authors are grateful to the Irish research council (GOIPG/2015/2952), Science foundation Ireland (12/IA/1414 and 13/IA/1896) and European research council (CoG 2014–647719) for the funding.

Notes and references

1 A. Caneschi, D. Gatteschi and R. Sessoli, *J. Chem. Soc., Dalton Trans.*, 1997, 3963-3970.
2 (a) C. M. Liu, R. G. Xiong, D. Q. Zhang and D. B. Zhu, *J. Am. Chem. Soc.*, 2010, **132**, 4044-4045; (b) Y. Zhang, W. Q. Liao, D. W. Fu, H. Y. Ye, Z. N. Chen and R. G. Xiong, *J. Am. Chem. Soc.*, 2015, **137**, 4928-4931.
3 D. Gatteschi, R. Sessoli and J. Villain, *Molecular Nanomagnets*, 2006.
4 (a) R. Sessoli, H. L. Tsai, A. R. Schake, S. Y. Wang, J. B. Vincent, K. Folting, D. Gatteschi, G. Christou and D. N. Hendrickson, *J. Am. Chem. Soc.*, 1993, **115**, 1804-1816; (b) R. Sessoli, D. Gatteschi, A. Caneschi and M. A. Novak, *Nature*, 1993, **365**, 141-143.
5 (a) A. K. Powell, S. L. Heath, D. Gatteschi, L. Pardi, R. Sessoli, G. Spina, F. Delgiallo and F. Pieralli, *J. Am. Chem. Soc.*, 1995, **117**, 2491-2502; (b) J. Larionova, M. Gross, M. Pilkington, H. Andres, H. Stoeckli-Evans, H. U. Gudel and S. Decurtins, *Angew. Chem. Int. Ed.*, 2000, **39**, 1605-1609; (c) Z. J. Zhong, H. Seino, Y. Mizobe, M. Hidai, A. Fujishima, S. Ohkoshi and K. Hashimoto, *J. Am. Chem. Soc.*, 2000, **122**, 2952-2953; (d) L. F. Jones, G. Rajaraman, J. Brockman, M. Murugesu, E. C. Sañudo, J. Raftery, S. J. Teat, W. Wernsdorfer, G. Christou, E. K. Brechin and D. Collison, *Chem. Eur. J.*, 2004, **10**, 5180-5194; (e) M. Murugesu, M. Habrych, W. Wernsdorfer, K. A. Abboud and G. Christou, *J. Am. Chem. Soc.*, 2004, **126**, 4766-4767; (f) A. M. Ako, I. J. Hewitt, V. Mereacre, R. Clerac, W. Wernsdorfer, C. E. Anson and A. K. Powell, *Angew. Chem. Int. Ed.*, 2006, **45**, 4926-4929; (g) T. C. Stamatatos, K. A. Abboud, W. Wernsdorfer and G. Christou, *Angew. Chem. Int. Ed.*, 2007, **46**, 884-888; (h) L. Zhang, R. Clérac, P. Heijboer and W. Schmitt, *Angew. Chem. Int. Ed.*, 2012, **51**, 3007-3011; (i) S. Kang, H. Zheng, T. Liu, K. Hamachi, S. Kanegawa, K. Sugimoto, Y. Shiota, S. Hayami, M. Mito, T. Nakamura, M. Nakano, M. L. Baker, H. Nojiri, K. Yoshizawa, C. Duan and O. Sato, *Nat. Commun.*, 2015, **6**; (j) L. Zhang, T. Chimamkpam, C. I. Onet, N. Zhu, R. Clérac and W. Schmitt, *Dalton Trans.*, 2016, **45**, 17705-17713.
6 (a) M. Hirahara, A. Shoji and M. Yagi, *Eur. J. Inorg. Chem.*, 2014, 595-606; (b) J. R. Carney, B. R. Dillon and S. P. Thomas, *Eur. J. Org. Chem.*, 2016, 3912-3929; (c) K. K. Krishnan, A. M. Thomas, K. S. Sindhu and G. Anilkumar, *Tetrahedron*, 2016, **72**, 1-16; (d) M. Perez-Navarro, F. Neese, W. Lubitz, D. A. Pantazis and N. Cox, *Curr. Opin. Chem. Biol.*, 2016, **31**, 113-119; (e) D. A. Valyaev, G. Lavigne and N. Lugan, *Coord. Chem. Rev.*, 2016, **308**, 191-235; (f) B. Maji and M. K. Barman, *Synthesis-Stuttgart*, 2017, **49**, 3377-3393; (g) R. Cano, K. Mackey and G. P. McGlacken, *Catal. Sci. Technol.*, 2018, **8**, 1251-1266; (h) D. C. Grills, M. Z. Ertem, M. McKinnon, K. T. Ngo and J. Rochford, *Coord. Chem. Rev.*, 2018, **374**, 173-217.
7 (a) B. Kok, B. Forbush and M. Mcgloin, *Photochem. Photobiol.*, 1970, **11**, 457-&; (b) H. Dau and M. Haumann, *Coord. Chem. Rev.*, 2008, **252**, 273-295; (c) J. Barber, *Chem. Soc. Rev.*, 2009, **38**, 185-196; (d) H. Dau and I. Zaharieva, *Acc. Chem. Res.*, 2009, **42**, 1861-1870; (e) J. Yano and V. Yachandra, *Chem. Rev.*, 2014, **114**, 4175-4205; (f) V. Krewald, M. Retegan and D. A. Pantazis, *Solar Energy for Fuels*, 2016, **371**, 23-48.
8 (a) J. E. McGrady and R. Stranger, *Inorg. Chem.*, 1999, **38**, 550-558; (b) W. Mtangi, V. Kiran, C. Fontanesi and R. Naaman, *J. Phys. Chem. Lett.*, 2015, **6**, 4916-4922; (c) V. Krewald, M. Retegan, F. Neese, W. Lubitz, D. A. Pantazis and N. Cox, *Inorg. Chem.*, 2016, **55**, 488-501; (d) J. Gracia, *Phys. Chem. Chem. Phys.*, 2017, **19**, 20451-20456; (e) W. Mtangi, F. Tassinari, K. Vankayala, A. Vargas Jentzsch, B. Adelizzi, A. R. A. Palmans, C. Fontanesi, E. W. Meijer and R. Naaman, *J. Am. Chem. Soc.*, 2017, **139**, 2794-2798; (f) J. Gracia, R. Sharpe and J. Munarriz, *J. Catal.*, 2018, **361**, 331-338; (g) F. A. Garcés-Pineda, M. Blasco-Ahicart, D. Nieto-Castro, N. López and J. R. Galán-Mascarós, *Nat. Energy*, 2019, **4**, 519-525.
9 (a) P. Christian, G. Rajaraman, A. Harrison, M. Helliwell, J. J. W. McDouall, J. Raftery and R. E. P. Winpenny, *Dalton Trans.*, 2004, 2550-2555; (b) T. Cauchy, E. Ruiz and S. Alvarez, *J. Am. Chem. Soc.*, 2006, **128**, 15722-15727; (c) J. Cano, T. Cauchy, E. Ruiz, C. J. Milios, C. C. Stoumpos, T. C. Stamatatos, S. P. Perlepes, G. Christou and E. K. Brechin, *Dalton Trans.*, 2008, 234-240; (d) C. Baffert, M. Orio, D. A. Pantazis, C. Duboc, A. G. Blackman, G. Blondin, F. Neese, A. Deronzier and M.-N. Collomb, *Inorg. Chem.*, 2009, **48**, 10281-10288; (e) E. Cremades, J. Cano, E. Ruiz, G. Rajaraman, C. J. Milios and E. K. Brechin, *Inorg. Chem.*, 2009, **48**, 8012-8019; (f) E. Cremades, T. Cauchy, J. Cano and E. Ruiz, *Dalton Trans.*, 2009, 5873-5878; (g) D. A. Pantazis, V. Krewald, M. Orio and F. Neese, *Dalton Trans.*, 2010, **39**, 4959-4967; (h) S. K. Singh, N. K. Tibrewal and G. Rajaraman, *Dalton Trans.*, 2011, **40**, 10897-10906; (i) N. Berg, T. Rajeshkumar, S. M. Taylor, E. K. Brechin, G. Rajaraman and L. F. Jones, *Chem. Eur. J.*, 2012, **18**, 5906-5918; (j) V. Krewald, F. Neese and D. A. Pantazis, *J. Am. Chem. Soc.*, 2013, **135**, 5726-5739; (k) T. Lohmiller, V. Krewald, M. P. Navarro, M. Retegan, L. Rapatskiy, M. M. Nowaczyk, A. Boussac, F. Neese, W. Lubitz, D. A. Pantazis and N. Cox, *Phys. Chem. Chem. Phys.*, 2014, **16**, 11877-11892; (l) K. R. Vignesh, S. K. Langley, K. S. Murray and G. Rajaraman, *Chem. Eur. J.*, 2015, **21**, 2881-2892; (m) T. Rajeshkumar, H. V. Annadata, M. Evangelisti, S. K. Langley, N. F. Chilton, K. S. Murray and G. Rajaraman, *Inorg. Chem.*, 2015, **54**, 1661-1670.
10 L. Zhang, B. Marzec, R. Clérac, Y. H. Chen, H. Z. Zhang and W. Schmitt, *Chem. Commun.*, 2013, **49**, 66-68.
11 M. J. T. Frisch, G. W.; Schlegel, H. B.; Scuseria, G. E.; Robb, M. A.; Cheeseman, J. R.; Scalmani, G.; Barone, V.; Mennucci, B.; Petersson, G. A.; Nakatsuji, H.; Caricato, M.; Li, X.; Hratchian, H. P.; Izmaylov, A. F.; Bloino, J.; Zheng, G.; Sonnenberg, J. L.; Hada, M.; Ehara, M.; Toyota, K.; Fukuda, R.; Hasegawa, J.; Ishida, M.; Nakajima, T.; Honda, Y.; Kitao, O.; Nakai, H.; Vreven, T.; Montgomery, J. A., Jr.; Peralta, J. E.; Ogliaro, F.; Bearpark, M.; Heyd, J. J.; Brothers, E.; Kudin, K. N.; Staroverov, V. N.; Kobayashi, R.; Normand, J.; Raghavachari, K.; Rendell, A.; Burant, J. C.; Iyengar, S. S.; Tomasi, J.; Cossi, M.; Rega, N.; Millam, J. M.; Klene, M.; Knox, J. E.; Cross, J. B.; Bakken, V.; Adamo, C.; Jaramillo, J.; Gomperts, R.; Stratmann, R. E.; Yazyev, O.; Austin, A. J.; Cammi, R.; Pomelli, C.; Ochterski, J. W.; Martin, R. L.; Morokuma, K.; Zakrzewski, V. G.; Voth, G. A.; Salvador, P.; Dannenberg, J. J.; Dapprich, S.; Daniels, A. D.; Farkas, Ö.; Foresman, J. B.; Ortiz, J. V.; Cioslowski, J.; Fox, D. J. , 2009.
12 F. Neese, *WIREs Comput. Mol. Sci.*, 2012, **2**, 73-78.
13 (a) J. P. Perdew, K. Burke and M. Ernzerhof, *Phys. Rev. Lett.*, 1996, **77**, 3865-3868; (b) C. Adamo and V. Barone, *J. Chem. Phys.*, 1999, **110**, 6158-6170.
14 M. Dolg, U. Wedig, H. Stoll and H. Preuss, *J. Chem. Phys.*, 1987, **86**, 866-872.
15 M. M. Francl, W. J. Pietro, W. J. Hehre, J. S. Binkley, M. S. Gordon, D. J. Defrees and J. A. Pople, *J. Chem. Phys.*, 1982, **77**, 3654-3665.
16 M. J. Frisch, J. A. Pople and J. S. Binkley, *J. Chem. Phys.*, 1984, **80**, 3265-3269.
17 H. B. Schlegel, *J. Comp. Chem.*, 1982, **3**, 214-218.
18 (a) A. P. Ginsberg, *J. Am. Chem. Soc.*, 1980, **102**, 111-117; (b) L. Noodleman, *J. Chem. Phys.*, 1981, **74**, 5737-5743; (c) L. Noodleman, D. A. Case and A. Aizman, *J. Am. Chem. Soc.*, 1988, **110**, 1001-1005; (d) E. Ruiz, J. Cano, S. Alvarez and P. Alemany, *J. Comp. Chem.*, 1999, **20**, 1391-1400.
19 R. Bauernschmitt and R. Ahlrichs, *J. Chem. Phys.*, 1996, **104**, 9047-9052.
20 (a) W. Heisenberg, *Z. Physik*, 1928, **49**, 619-636; (b) P. A. M. Dirac, *Proc. R. Soc. Lond. A*, 1929, **123**, 714-733; (c) J. H. Vanvleck, *Rev. Mod. Phys.*, 1945, **17**, 27-47.

View Article Online
DOI: 10.1039/D0DT01404D

21 S. Paul and A. Misra, *J. Chem. Theory Comput.*, 2012, **8**, 843-853.
22 (a) R. S. Mulliken, *J. Chem. Phys.*, 1955, **23**, 1833-1840; (b) R. S. Mulliken, *J. Chem. Phys.*, 1955, **23**, 2343-2346; (c) R. S. Mulliken, *J. Chem. Phys.*, 1955, **23**, 1841-1846; (d) R. S. Mulliken, *J. Chem. Phys.*, 1955, **23**, 2338-2342; (e) F. L. Hirshfeld, *Theoret. Chim. Acta*, 1977, **44**, 129-138; (f) J. P. Ritchie, *J. Am. Chem. Soc.*, 1985, **107**, 1829-1837; (g) J. P. Ritchie and S. M. Bachrach, *J. Comp. Chem.*, 1987, **8**, 499-509; (h) R. F. W. Bader, 1990; (i) M. Yu and D. R. Trinkle, *J. Chem. Phys.*, 2011, **134**.
23 E. Ruiz, T. Cauchy, J. Cano, R. Costa, J. Tercero and S. Alvarez, *J. Am. Chem. Soc.*, 2008, **130**, 7420-7426.
24 https://github.com/WatsonGroupTCD/EJ_Calc).
25 O. Kahn, *VCH Publishers, Inc.(USA), 1993*, 1993, 393.
26 F. Neese, *J. Chem. Phys.*, 2005, **122**.
27 N. F. Chilton, R. P. Anderson, L. D. Turner, A. Soncini and K. S. Murray, *J. Comp. Chem.*, 2013, **34**, 1164-1175.
28 https://github.com/WatsonGroupTCD/Suscep).
29 M. Shoji, K. Koizumi, Y. Kitagawa, T. Kawakami, S. Yamanaka, M. Okumura and K. Yamaguchi, *Chem. Phys. Lett.*, 2006, **432**, 343-347.
30 (a) C. Adamo, M. Cossi and V. Barone, *THEOCHEM*, 1999, **493**, 145-157; (b) E. V. Gorelik, V. I. Ovcharenko and M. Baumgarten, *Eur. J. Inorg. Chem.*, 2008, 2837-2846.
31 M. G. Medvedev, I. S. Bushmarinov, J. W. Sun, J. P. Perdew and K. A. Lyssenko, *Science*, 2017, **355**, 49-52.
32 (a) J. B. Goodenough, *J. Phys. Chem. Solids*, 1958, **6**, 287-297; (b) J. Kanamori, *J. Phys. Chem. Solids*, 1959, **10**, 87-98.

View Article Online
DOI: 10.1039/D0DT01404D

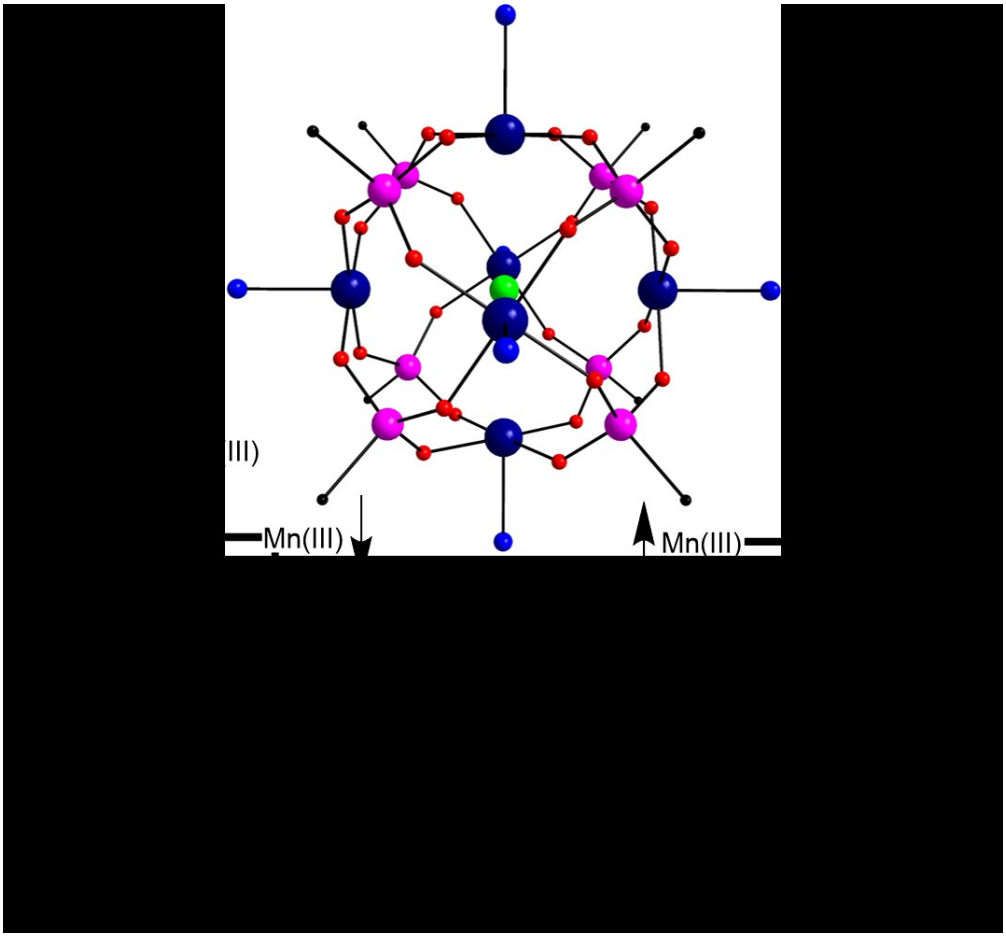

45x42mm (600 x 600 DPI)